INORGANIC CHEMISTRY
FRONTIERS

RESEARCH ARTICLE

View Article Online
View Journal | View Issue

Check for updates

Cite this: *Inorg. Chem. Front.*, 2023, **10**, 1511

Exfoliating layered zeolite MFI into unilamellar nanosheets in solution as precursors for the synthesis of hierarchical nanocomposites and oriented films†

Wieslaw J. Roth, *[a] Takayoshi Sasaki, *[c] Karol Wolski, [a] Barbara Gil, [a] Szczepan Zapotoczny, [a] Jiří Čejka, [b] Martin Kubů, [b] Michal Mazur, [b] Yasuo Ebina, [c] Nobuyuki Sakai, [c] Dai-Ming Tang [c] and Renzhi Ma [c]

Zeolites have many uses and are continually developed for catalysis and separations as highly active, selective and thermally stable materials with microporous framework structures of various topologies. Among approximately 250 known frameworks about 20, but possibly all eventually, produced 2D forms with layers of thickness up to a few nanometers. Recently, layered forms of the zeolite MWW and a ferrierite-related one have been exfoliated directly by a soft-chemical treatment into solutions of unilamellar nanosheets. They enable the synthesis of layer-based hierarchical and nanocomposite materials with diverse compositions that are unfeasible with solid 3D and 2D forms. The efficiency and yield of zeolite exfoliation can be inhibited by intergrowth so each topology presents a separate challenge. The MFI zeolite can provide particular benefits as one of the most active and versatile frameworks. It has permeable layers due to perpendicular channels and has been used as a membrane. This article describes exfoliation of the layered MFI produced by the bifunctional template developed by Ryoo *et al.* It affords unilamellar MFI nanosheets in solution with a uniform hydrated thickness of 3.6 nm confirmed by AFM, X-ray diffraction and TEM. The nanosheets can be reassembled top-down into self-standing *b*-oriented discs or films, proven by X-ray powder diffraction. They preserve high acid site concentration and porosity. The basal spacing contracts from 3.6 nm to 2.8 nm upon calcination. Oriented MFI films were also formed by the evaporation/calcination of nanosheet solutions and surfactant composites enabling simple fabrication on various substrates for application in catalysis and separations.

Received 26th October 2022,
Accepted 11th January 2023

DOI: 10.1039/d2qi02283d

rsc.li/frontiers-inorganic

Open Access Article. Published on 27 Januar 2023. Downloaded on 09.10.2025 04:40:51.
This article is licensed under a Creative Commons Attribution 3.0 Unported Licence.

Introduction

Aluminosilicate zeolites and related molecular sieves are generally known and applied in practice as crystalline materials with microporous framework structures that show exceptional benefits as catalysts, selective sorbents and ion exchangers.[1–3] They contain uniform micropores, typically less than 1 nm, in combination with strong acid sites.[4,5] Zeolites are used in various industrial processes,[6–8] and are continuously developed for further expansion especially as eco-oriented applications.[9,10] There are now over 250 known zeolite topologies but only about 20 of them have been developed technologically.[11] Originally zeolites were found in only one form, a rigid immutable framework extended in all three dimensions. In a surprising twist it was found that the same structure can produce a second form, 2-dimensional layers with thickness of up to a few nanometers.[12–14] In one embodiment these layers can be stacked as semi-ordered (layered) precursors and upon heat treatment they condense to produce the corresponding complete frameworks.[12,15,16] Unlike the original rigid 3D forms, the layered 2D zeolites have flexible structures that can be modified, especially to provide expanded or re-organized materials.[17–20] Recently two of the layered zeolites, MWW and a ferrierite-related one denoted as bifer, have been completely separated into monolayers in solution by soft-chemical exfoliation with tetrabutylammonium hydroxide (TBAOH). They produced suspensions of unilamellar nanosheets in solution[21–23] effectively as a third zeolite form, which enables unpre-

[a]*Jagiellonian University, Faculty of Chemistry, Gronostajowa 2, 30-387 Kraków, Poland. E-mail: wieslaw.roth@uj.edu.pl*
[b]*Department of Physical and Macromolecular Chemistry, Faculty of Science, Charles University, Hlavova 8, 12840 Prague 2, Czech Republic*
[c]*International Centre for Materials Nanoarchitectonics (WPI-MANA), National Institute for Materials Science (NIMS), 1-1 Namiki, Tsukuba, Ibaraki 305-0044, Japan. E-mail: sasaki.takayoshi@nims.go.jp*
† Electronic supplementary information (ESI) available. See DOI: https://doi.org/10.1039/d2qi02283d

Open Access Article. Published on 27 Januar 2023. Downloaded on 09.10.2025 04:40:51.
This article is licensed under a Creative Commons Attribution 3.0 Unported Licence.

cedented synthetic opportunities as a homogeneous liquid phase reagent. In Fig. 1 the 3 different zeolite forms have been compared and the unique synthetic possibilities enabled by the zeolite layers in solutions have been highlighted.

Zeolite nanosheets in solution can be used in synthesis as nanosized building blocks, individually or with other functional components, to generate diverse composite and hierarchical materials that were unfeasible before with the 3D form and even with solid 2D forms.[24] Illustrative examples include mixed zeolite layers exemplified by already obtained MWW and bifer composites,[21] intimate composites of layers with nanoparticles (unpublished) and oriented disks,[22] as shown in Fig. 1. The separation of 2D zeolites into single layers is commonly referred to as delamination and initial attempts relied on pre-expansion with surfactants (swelling). There had been no indications nor proof of layer dispersion into a solution by direct or simple treatments, like ultrasonication, in any of the previous reports.[25–30] In one study, zeolite layers of MWW and MFI coated with surfactants were indeed dispersed into monolayer nanosheets in solution but through a multi-step process using twin-screw extrusion. It produced very low yields of the dispersed layers, which together with the surfactant coating and complicated preparation methodology presented very limited options for post-synthetic exploitation.[23,29]

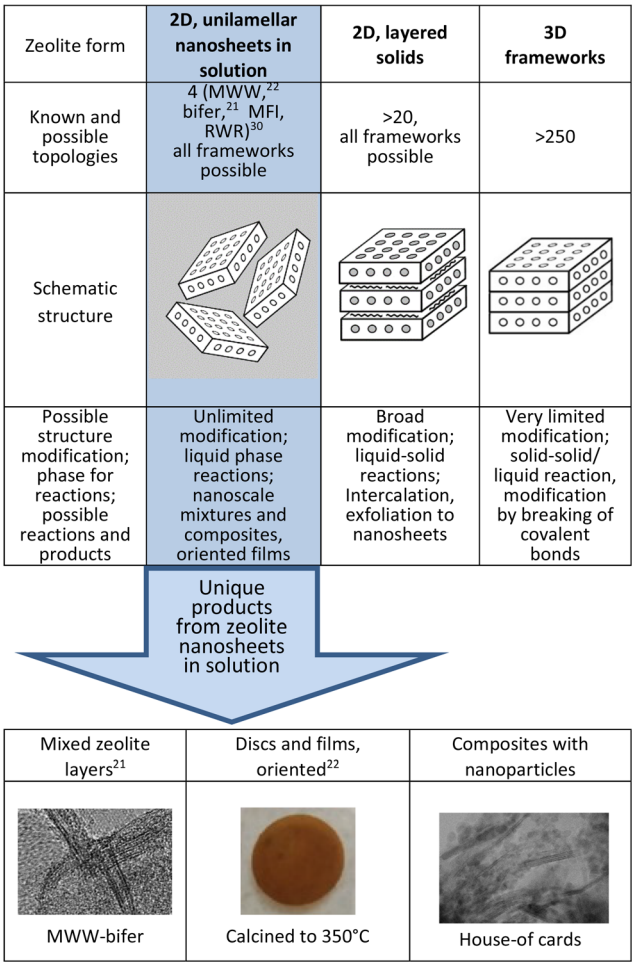

Fig. 1 Three different zeolite forms, the number of known topologies for each, and modification potential with examples of unique products enabled by the nanosheets dispersed in solution.

There are two most prominent and valuable zeolites, FAU and MFI, but only the latter is available in a 2D form, so its exfoliation has a particular importance. Additionally, MFI layers have perpendicular channels of roughly 0.5 nm diameter, which may provide extra benefits in catalysis and membrane-like separations.[31] The zeolite layers exfoliated to date, MWW, bifer and RWR, are impermeable. The treatment with TBAOH solutions provides a convenient and direct method of exfoliation but the yield depends on the zeolite synthesis method, *i.e.*, gel composition and conditions, in a way that is not well understood yet. Presumably, the layers can intergrow and limit the complete separation potential. This should be minimized during hydrothermal synthesis but the controlling factors are unknown. In short, the successful exfoliation of MFI and additional zeolites in meaningful yields depends on identifying suitable preparations.

Layered MFI materials can be obtained by the method invented by Ryoo *et al.*[32] It uses bifunctional templates with long hydrocarbon tails that prevent structure continuation in the 3rd dimension during synthesis. These templates are integrated into the layer but the tails line the surface and inhibit interaction with TBAOH, thus preventing exfoliation. We resolved this problem by thermal degradation of the organics at 350 °C. The final yields of exfoliated MFI layers are lower than that of the previous two cases, MWW and bifer, but it is still a significant advance as a demonstration and it enables film fabrication. Increasing the yield will be a matter of finding a more suitable synthetic procedure for the starting layered MFI. This report has two parts. The first describes the exfoliation of MFI into solutions of unilamellar nanosheets and the confirmation based on atomic force microscopy (AFM), X-ray powder/film diffraction (XRD) and electron microscopy. The second part focuses on proving the formation of oriented films that can show the usefulness and novel practical potential, *e.g.*, for sieving and catalytic applications.[31] Zeolites available as layers in solution can be considered for the development of advanced applications, where polycrystalline forms are less useful. Specific examples include membrane separations, low-*k* materials, protective coating and sensing.[33] Structured zeolite materials prepared *via* exfoliation can be also useful for the investigation of fundamental catalytic and mass transport properties.

Results and discussion

The structure of zeolite MFI and the thickness of its layer are discussed first because of the ambiguity of the latter, since both 1- and 1.5-unit cell values have been cited for apparently equivalent materials.[23,32,34]

This journal is © the Partner Organisations 2023

Open Access Article. Published on 27 Januar 2023. Downloaded on 09.10.2025 04:40:51.
This article is licensed under a Creative Commons Attribution 3.0 Unported Licence.

Structure and thickness of MFI layers

The framework of the zeolite MFI shown in Scheme 1 is generated by the stacking and fusion of pentasil slabs along the crystallographic *b* direction.[35] The formal unit cell along *b* contains 2 such slabs and the corresponding lattice constant (*b*-axis) is equal to 2 nm. This generates two types of channels: straight 10-rings with an approximate diameter of 0.5 nm in the *b* direction (vertical) and sinusoidal in the *a* direction (horizontal, perpendicular). Layers are terminated in the regions of reduced framework density, which in this case is between the slabs but it is not evident how many slabs per layer can be expected. This seems to be determined by the structure directing agents (SDA, template), which are designed to have (i) head groups that template the layers and remain in the pores and (ii) long hydrocarbon chains protruding outside, lining the surface, and preventing structure propagation in the 3rd dimension during growth. The corresponding bifunctional templates (SDAs) have a general formula $RN(CH_2)_nNC_mH_{2m+1}$, with +2 charge. The most common SDA, which is also used in this work has R = $C_{22}H_{45}$, and n and m equal to 6; it is designated C22-6-6. The typical as-synthesized product is multilayered with a basal spacing of *ca.* 6 nm, indicated by a strong 010 reflection in the XRD, resulting from stacked MFI layers separated by the organic region. The exact thickness of each region is hard to determine directly. MFI zeolite layers are typically seen with two rows of pores in the cross-sectional view in TEM.[32,34] As shown in Scheme 1 this is produced by 3 pentasil slabs and corresponds to 1.5-unit cells with approximate overall theoretical (anhydrous) thickness of around 3 nm.[23,34] This fusion of 3 slabs to produce an MFI layer has been rationalized based on the packing of the templates.[34] The same thickness is observed in the MFI nanosheets studied herein and was also determined in the prior work on MFI delamination.[23] Isolated MFI nanosheets produce typical MFI powder XRD patterns, even when disorganized, identified by prominent doublets at 2θ values of 8–9° and near 23° (Cu Kα radiation, used throughout unless specified otherwise). This allows easy and instantaneous identification as shown in Fig. 2. More detailed analysis and assignments are discussed later in connection with the oriented films.

MFI exfoliation with tetrabutylammonium hydroxide (TBAOH)

The reported earlier exfoliation of MWW and bifer as unilamellar nanosheets in solution occurred through the direct treatment of the as-synthesized samples with TBAOH solutions. The as-synthesized MFI with surfactant templates embedded

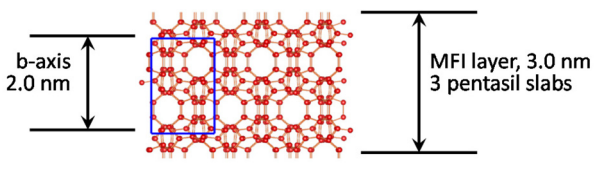

Scheme 1 Structure of the MFI zeolite as the stacking of pentasil slabs viewed along the [100] axis with the unit cell shown in blue.

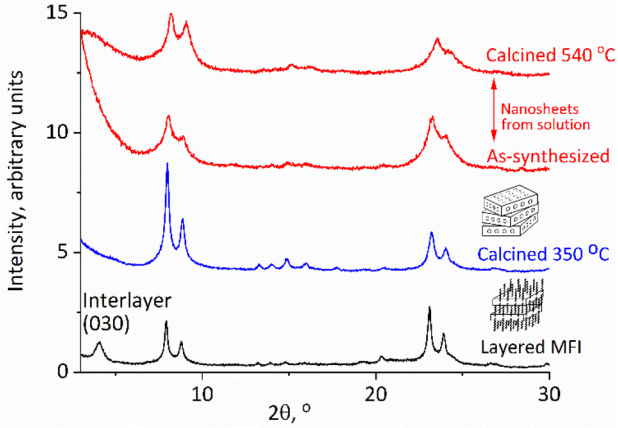

Fig. 2 XRD patterns of the as-synthesized layered MFI (bottom), calcined at 350 °C (second from bottom), and exfoliated nanosheets recovered by acidification, uncalcined, and calcined (top).

in the layers and hydrocarbon tails lining the surface did not exfoliate directly with TBAOH, so the idea was to remove the excess organic first. As mentioned above, the previous attempts at dispersing MFI layers into solutions employed a multistep procedure with the template left in, which involved: melt-blending with polymers in a screw extruder, extraction and purification.[23] The yield of dispersed MFI layers was low and probably insufficient for more general use in synthesis. The remaining embedded surfactant was removed by oxidation with the piranha solution as the last step.[23] Our approach involved the elimination of the surfactant tails by thermal degradation, which had to be performed at a relatively low temperature and 350 °C was chosen based on TG-DTG, as shown in ESI Fig. S1,† to minimize condensation of surface silanols and layer crosslinking. This produced a red-brown solid with less than 5% of the residual coke (average content N 0.46%, C 3.82% and H 0.36%). The XRD patterns showed a structural contraction from 6 nm to *ca.* 3 nm as shown in Fig. 2. The original as-synthesized MFI with the template shows reflections at a 2θ value of 1.4° (not shown) and 4.2° (corresponding to 6 nm and 2 nm *d*-spacing and 010 and 030 indices) and also the characteristic peaks for MFI, *i.e.*, the doublets at 2θ value of 8–9° and near 23° as mentioned above. After being heated at 350 °C the low angle basal reflections disappeared but the pattern resembled that of a typical MFI with reflections above 8°, matching those of the standard MFI and the starting material, with an increased intensity (Fig. 2). These pre-calcination conditions were the same for all preparations but there may be room for the optimization of the temperature and other conditions, especially if preparations affording higher exfoliation yields can be identified.

The exfoliation was started by mixing the solid with 10% TBAOH in water for a few hours and centrifuging at 10 000 rpm. All solids were flocculated due to the high ionic strength, and after the decantation of the supernatant, they were mixed with water. The slurry was centrifuged again producing the nanosheets in solution as confirmed below. This cycle of water

Open Access Article. Published on 27 Januar 2023. Downloaded on 09.10.2025 04:40:51.
This article is licensed under a Creative Commons Attribution 3.0 Unported Licence.

addition, centrifugation and decantation can be repeated several times to increase the recovery of the MFI nanosheets in an amount of 50–100 mg when starting with 0.5 to 1 g of the layered zeolite (MWW and bifer could be obtained in yields up to 70% in the second step alone). The obtained MFI nanosheets in solution could be isolated for characterization and practical use by acidification, micro-filtration or flocculated with cations, as elaborated below. When isolated as solids they produce MFI-like XRD patterns as shown in Fig. 2. As shown below, they also exhibit acidic properties and porosity typical of an MFI.

Subsequent characterization confirmed that the nanosheets have a uniform thickness based on the 3 nm inorganic core, *i.e.*, 1.5×*b*-axis of the MFI, with variations due to hydration and related phenomena. These characterization studies include AFM followed by in-plane XRD and TEM, from which the MFI structure was confirmed. The uniform unilamellar thickness of the layers was also revealed in their products, especially the oriented films, individually and as composites with surfactants, as described below.

Determining uniform layer thickness by AFM

AFM imaging confirmed the uniform thickness of the nanosheets in solution after they were spin-cast on a silicon wafer modified by coating with positively charged polyethyleneimine (PEI). The analyzed images, presented in Fig. 3(a–c), show that majority of the layers are roughly 3.6 nm thick, as highlighted by the cross-section height profiles (Fig. 3c). The complete analysis was carried out by the calculation of the height histogram (Fig. 3d) generated from five AFM topography images captured in different places on the sample surface. The histogram in Fig. 3d shows 2 distinct maxima at 0.0 (support) and 3.6 nm. The latter was adopted as the average hydrated layer thickness value. It matches with the value of 3.4 ± 0.3 nm reported previously,[23] and is consistent with the recognized 1.5 unit cell thickness of the MFI layers, and not one unit cell thickness that is often assigned in the literature. The images also show sporadic regions of higher thickness. The total contribution of the objects thicker than 4.5 nm, estimated from the histogram, is 12–13% of all structures observed on the surface. The thicker particles can be layers connected due to association or successive deposition, or unexfoliated integrated fragments. The planar dimensions of the observed nanosheets are in the range of tens to several hundred nanometers.

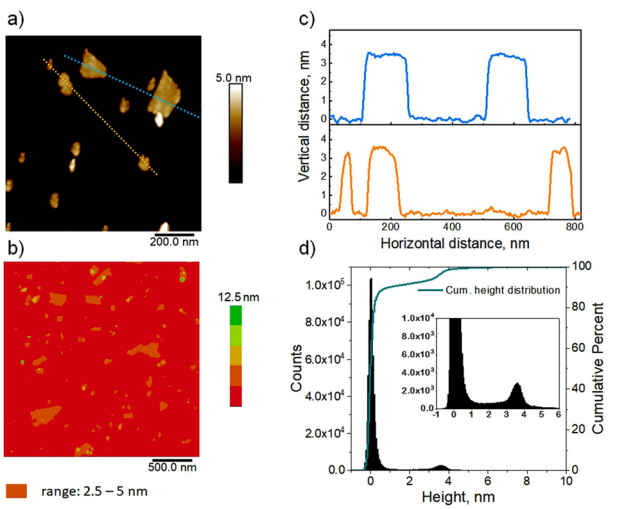

Fig. 3 AFM topography images of the MFI nanosheets deposited on PEI modified silicon wafers (a and b); cross-section height profiles along the marked dotted lines in the topography image a (c); the height histogram with cumulative height distribution generated from five AFM images captured in various places on the sample surface, including the 0 level, and an inset highlighting the dominant 3.6 nm height (d).

In-plane XRD and TEM of exfoliated layers

In-plane XRD generates only *h0l* reflections, which can provide the *a*–*c* planar dimensions. Fig. 4 shows the XRD pattern after the pre-processing of the synchrotron data as discussed in detail in the Experimental section. All visible peaks could be indexed based on a 2D rectangular unit lattice with refined cell parameters of 2.006(2) × 1.340(1) nm^2. These values match with the unit cell of the precursor MFI phase, indicating that the MFI host framework was preserved upon exfoliation and being transferred into solution.

TEM evaluation, presented in Fig. 5, provides details of the layered structure, and confirms the MFI topology based on the corresponding crystallographic parameters and pores. The low-

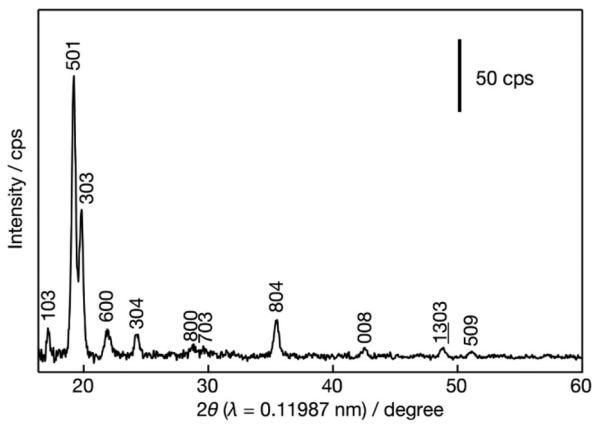

Fig. 4 In-plane XRD for MFI nanosheets.

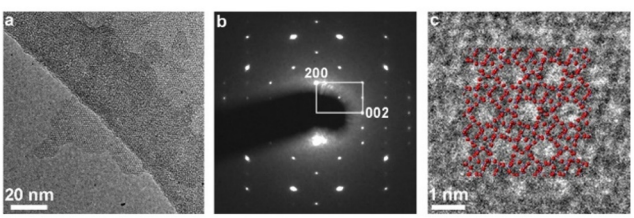

Fig. 5 TEM imaging of the layers. (a) Low-magnification TEM image, (b) selected area electron diffraction (SAED) pattern, and (c) high-resolution TEM image of a nanosheet with in-plane orientation.

This journal is © the Partner Organisations 2023

Open Access Article. Published on 27 Januar 2023. Downloaded on 09.10.2025 04:40:51.
This article is licensed under a Creative Commons Attribution 3.0 Unported Licence.

magnification TEM image (Fig. 5a) reveals a regular porous pattern, extending to the whole nanosheet with a size of around 100 nm. The selected area electron diffraction (SAED) pattern (Fig. 5b) could be indexed as a single crystalline MFI structure along the [010] zone axis with approximate lattice constants (d_{200} ~ 1.06 nm and d_{002} ~ 0.69 nm with ~90° angle). The high-resolution TEM (HRTEM) image of the in-plane structure (Fig. 5c) is overlapped with the atomic model and shows their congruence in the pore arrangement and the atomic framework.

Edge-on images shown in Fig. 6 were obtained with oriented discs that are discussed in the next section.

Oriented MFI films

The solutions obtained by the above procedure could be filtered under vacuum to produce discs or films, *e.g.*, with a diameter of 1.5 cm.[22,29] A Millipore glass filtration set (25 mm diameter) was used with filters of pore sizes down to 0.025 μm. This produced regular self-standing discs, as shown in Fig. 1, bottom, which could be calcined at 540 °C and ion-exchanged with ammonium nitrate to obtain acid forms for quantitative evaluation by FTIR (*vide infra*). The as-synthesized films are typically red-brown due to organic coke but turn white or clear by calcination at 540 °C. Their identity was confirmed first by XRD after calcination, which showed patterns indicating the MFI structure with perpendicular *b*-axis orientation.

Given the high aspect ratio of zeolite layers it is natural to expect their oriented packing face-to-face upon multilayer deposition, *e.g.*, during filtration, but the anticipated *b*-orientation must be confirmed. The evidence is provided by the XRD pattern of a calcined disc, presented in Fig. 7. The calcined disc or film (top two patterns in Fig. 7) shows only the second of the two principal MFI reflections with 2θ values at 8° and 8.9° (Fig. 7, second plot from the bottom). Because in a *b*-oriented film only 0*k*0 reflections should be visible, the first one, at a 2θ value of 8°, assigned to 101/011, must be extinct, while the second, at a 2θ value of 8.9°, combining the 200 and 020 reflection, should remain. This is indeed the case here, as shown in Fig. 7, in agreement with the literature.[36] There is an additional scattering at around a 2θ value of 23°, which may be related to the prominent high intensity doublet at 2θ values of 23.2° and 23.8° (501, 051 and 151, 303, respectively) of the regular MFI. These reflections are not expected to be visible so

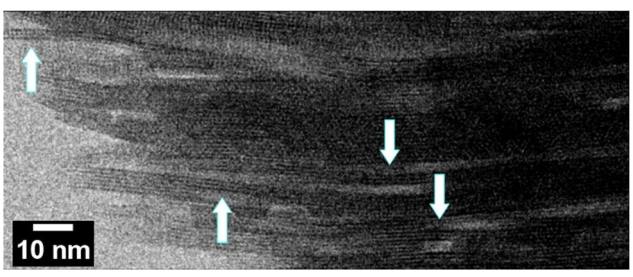

Fig. 6 The edge-on STEM-ABF image of an MFI disc. Arrows point to single MFI layers, 3 nm thick with clearly observed two rows of pores.

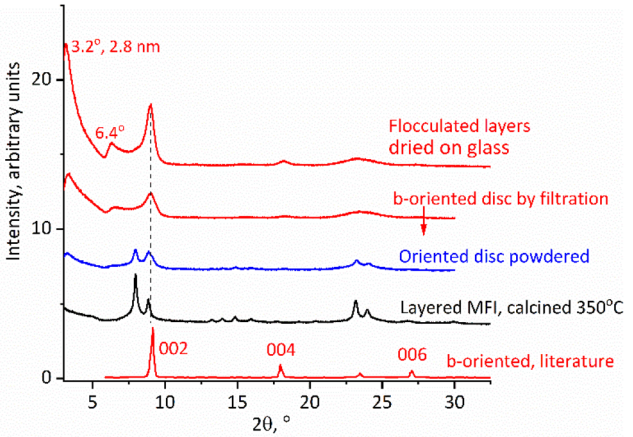

Fig. 7 XRD patterns of calcined MFI discs, *b*-oriented highlighted in red, compared to polycrystalline layered MFI. The literature pattern was adapted with permission from ref. 36 (Z. Wang *et al.*, Fabrication of a Highly b-Oriented MFI-Type Zeolite Film by the Langmuir–Blodgett Method, *Langmuir*, 2014, **30**, 4531–4). Copyright 2014 American Chemical Society.

the observation of this scattering may indicate some deviation from the ideal *b*-orientation in some parts of the film, but other explanations or unknown effects cannot be ruled out. In fact, the literature pattern shown in Fig. 7 also shows a small peak in this region.[36]

The calcined MFI discs exhibited additional highly asymmetric peaks in the XRD spectra (Fig. 7) located below a 2θ value of 8° at 2θ values of 3.2° and 6.4° with *d*-spacings of 2.8 and 1.4 nm. Such peaks are usually not observed for the MFI structure but in this case can be explained as 010 and 020 reflections produced by stacking of the MFI layers with an interlayer repeat distance equal to 2.8 nm. This value is shorter than the recognized layer thickness equal to 3 nm but there is no contradiction here. The latter thickness is based on layers aligned and connected by vertical Si–O–Si bridges. Exfoliated layers are expected to stack without alignment resulting in SiOH groups located in troughs or indentations in the surface such as pore openings. This can decrease an apparent thickness and has been observed before with other zeolites resulting in materials called sub-zeolites[37] because their interlayer *d*-spacing is shorter than the layer thickness determined on the basis of 3D structures with Si–O–Si bridges. As an alternative assignment two low angle peaks were considered together with a reflection at a 2θ value of 8.9° as possible 010, 020 and 030 orders of the same basal spacing, *i.e.*, 2.8 nm. This was dismissed because the determined position of the last reflection, at a 2θ value of 8.9°, deviated too much from the expected 2θ value of 9.6°. Secondly, the peaks at 2θ values of 3.2 and 6.4° have a similar asymmetric shape that is completely different from the 3rd peak at a 2θ value of 8.9°. The former have a tail on the right side, which may be caused by fluctuations in the horizontal interlayer distances as recognized with clays.[38] The corresponding XRD patterns of the discs before calcination contain related low angle peaks but

Open Access Article. Published on 27 Januar 2023. Downloaded on 09.10.2025 04:40:51.
This article is licensed under a Creative Commons Attribution 3.0 Unported Licence.

the interlayer distance is larger, 3.6 nm, and contracts to 2.8 nm upon calcination, which is discussed in the next paragraph.

Table 1 provides a summary of the XRD pattern analysis with assigned interplanar spacings and peak positions.

XRD patterns of the as-synthesized discs/films are dominated by low angle peaks roughly at 2θ intervals of 2.5° with apparent orders of a 3.6 nm basal spacing. Additional smaller maxima also appear as multiples of the 2θ interval of 2.5° up to the 2θ value of 27.5° suggesting an oriented packing with a roughly 3.6 nm repeating unit that is consistent with the thickness of monolayers observed in AFM. This expansion is caused by the additional water and intercalated organic layer, which are removed upon calcination, accompanied by a color change from brown to colorless or white and a contraction to the 2.8 nm repeat discussed above. As with the calcined disc, there is also an additional pronounced scattering with a maximum 2θ of around 23°, roughly corresponding to the most intense reflections for the MFI. In the as-synthesized XRD pattern, the 020 peak at the 2θ value of 8.9°, characteristic for the MFI structure and the most prominent in the calcined form, is barely visible if at all. This underscores the need for calcination to prove the preferred orientation layer.

The obtained exfoliated layers in solution can also produce oriented films on being dried on a flat surface directly or after flocculation as solids. A particularly notable case is that of the films being produced by solids precipitated with cationic surfactants such as hexadecyltrimethylammonium. They have an expanded 'swollen' structure with a basal spacing of 6 nm (interlayer gallery of 3 nm), which is revealed after deposition and drying on a flat surface. They are discussed in the next section.

b-Oriented surfactant-MFI films with expanded basal spacings

The solutions of exfoliated MFI layers produce precipitates upon mixing with surfactants such as hexadecyltrimethylammonium cations (HDTMA). These products are multilayer composites akin to surfactant-swollen zeolites,[39] with a regular interlayer spacing of approximately 6 nm. Their structural features were revealed in the XRD of the samples obtained by depositing slurries on glass slides followed by drying, and eventually calcination.

XRD patterns of the dried MFI-surfactant precipitate, presented in Fig. 8 top, 2nd from the bottom, show 3 orders of 0*k*0 reflections at *ca.* 2θ intervals of 1.6°, which correspond to an interlayer *d*-spacing of 5.7 nm. The 010 reflection is particularly intense. After calcination, the XRD pattern is the same as that for the calcined disc with *b*-oriented layers obtained by vacuum filtration showing a basal spacing of 2.8 nm. This proves a strict *b*-orientation that is preserved despite 50% basal contraction upon calcination, which is hard to expect *a priori* but can be rationalized by a high aspect ratio of the layers that maintains their face-to-face orientation. This is significant as an illustration of the possibility for preparation of oriented films by simple deposition from suspensions and drying/calcination, which may allow a convenient larger scale film manufacture.

Acid and textural properties of MFI discs

The preservation of unique MFI qualities, *viz*. acidity and porosity, during preparation and processing is essential for the effective usage of the films in practical application. This was confirmed by FTIR and gas adsorption studies, respectively.

Table 1 Summary of important XRD peak positions for MFI and its layered derivatives

	MFI layers	MFI layers with hexadecyltrimethylammonium cation
Basal spacing, nm (° 2θ Cu Kα)		
As-synthesized film	3.6 nm (2.5°)	5.7 nm (1.6°)
Calcined film	2.8 nm (3.2°)	2.8 nm (3.2°)
Layer thickness anhydrous	3.0 nm (1.5-unit × 2.0 nm)	
020 peak MFI	1.0 nm (8.9°)	1.0 nm (8.9°)
Observed selected reflections, ° 2θ Cu Kα		
As-synthesized film	2.5° intervals	1.6° intervals
Calcined film	3.2, 6.4, 8.9°	3.2, 6.4, 8.9°
Layered powder, as-synthesized	1.4, 4.2, 8.0, 8.9°	
Layered powder, calcined	8.0, 8.9°	

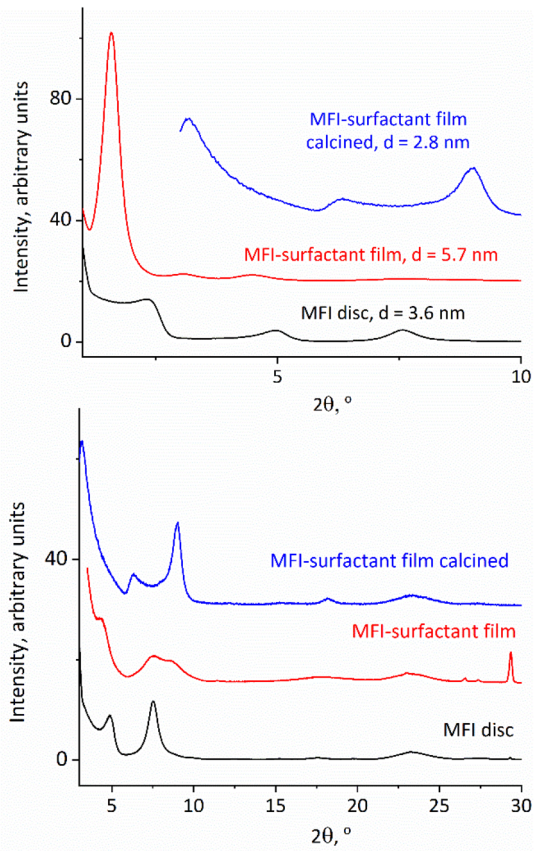

Fig. 8 Low angle (top) and high angle (bottom) XRD patterns for as-synthesized and calcined films of surfactant-flocculated MFI layers compared to an as-synthesized MFI disc.

This journal is © the Partner Organisations 2023

Open Access Article. Published on 27 Januar 2023. Downloaded on 09.10.2025 04:40:51.
This article is licensed under a Creative Commons Attribution 3.0 Unported Licence.

The discs obtained *via* filtration were calcined at 540 °C and statically ammonium exchanged by immersing 2–3 times in 1 M ammonium nitrate solution for a few hours and repeated washing with water. The results are presented in Table 2. There is no change in the BAS (Brønsted acid sites) and LAS (Lewis acids sites) concentration in comparison to the original zeolite powder, proving viability for catalysis.

Similarly, nitrogen adsorption studies showed that the micropores were also preserved despite various treatments (Table 2). Especially notable is the hysteresis loop at $p/p^0 > 0.4$ as shown in Fig. 9. It suggests slit-like pores, consistent with SEM images shown below, with an increased accessibility, which can be conducive to an enhanced interaction with bulky molecules.

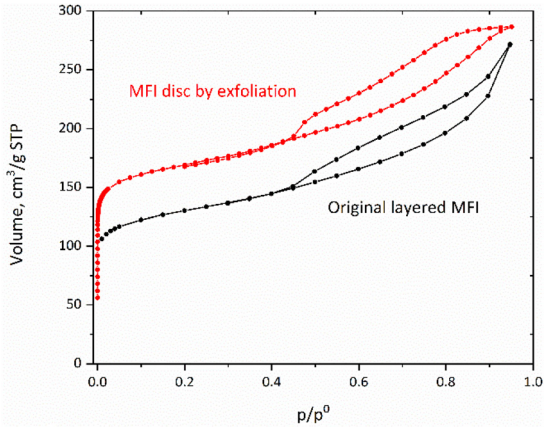

Fig. 9 Nitrogen sorption isotherms for the original layered MFI and an MFI disc (shifted vertically by 50 $cm^3\ g^{-1}$).

SEM and STEM-ADF images of the MFI discs

Structure of the discs is revealed by SEM and TEM images shown in Fig. 10. The SEM images show relatively uniform thickness of the disc equal to approximately 30 μm, controllable during the preparation, and macroscopic smoothness without excessive defects. Its layered structure is observed in the close-up cross-sectional view shown in Fig. 10c, but it is uncertain if the observed features represent individual layers. The latter have been revealed by STEM-ABF (Fig. 6 and 10d–f). Fig. 6 shows stacks of aligned porous layers, not ideally but with minor bends and discontinuities. Parts of single nanosheets with 3 nm thickness can be discerned in some places as pointed by arrows. In STEM, Fig. 10d–f, individual nanosheets of approximately 3 nm thickness can be discerned. These images show stacking of the layers (white strips) but with gaps visible as darker parts that suggest slit-shape voids. They are consistent with the interlayer mesopores observed by nitrogen sorption. SEM of the original MFI is provided in the ESI, Fig. S2.†

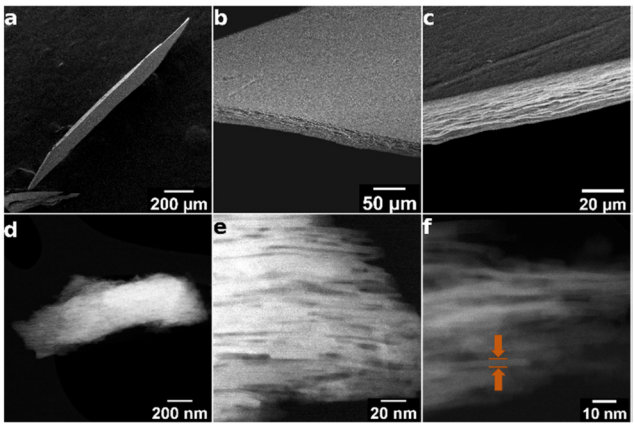

Fig. 10 Images of the fragments of the MFI disc obtained *via* exfoliation: top, SEM of a self-standing zeolite film: (a) the macroscopic view of the disc fragment, (b) closeups highlighting uniform thickness and surface homogeneity of the film, (c) cross-section showing layers of packing in the film. Bottom, STEM-ADF images of self-standing MFI zeolite films, edge-on view: (d) general fragment of a film, (e) closeup showing the arrangement of layers, (f) a high-resolution image with the indicated MFI single-layer.

Significance and uses of (oriented) zeolite films

Solutions of zeolite monolayers and films that can be readily produced with them provide opportunities to develop zeolites in new directions beyond those possible or contemplated with

Table 2 Concentrations of Brønsted (BAS) and Lewis (LAS) acid sites and textural properties of the layered MFI and an oriented disc produced *via* exfoliation

	Acid site concentration, μmol g^{-1}				Si/Al, mol/mol	
MFI zeolite form	BAS	LAS	BAS + LAS	BAS, %	BAS+LAS	BAS
Original layered	550	147	697	79	23	29
Disc	571	110	681	84	24	28

Textural properties

	Surface area, $m^2\ g^{-1}$			Pore volume, $cm^3\ g^{-1}$	
MFI type	BET	Micropore *t*-plot	Mesopore *t*-plot	Micropore *t*-plot	Single point at 0.95 p/p_0
Disc	411	223	181	0.105	0.367
Original layered	447	280	167	0.130	0.420

Open Access Article. Published on 27 Januar 2023. Downloaded on 09.10.2025 04:40:51.
This article is licensed under a Creative Commons Attribution 3.0 Unported Licence.

the conventional polycrystalline 3D or 2D forms. The promising areas include tailoring of the surface activity with particular active centers (metals) and functional groups, membrane-like transport and separations, nanoscale insulation, in optical, electric, *etc*. applications as supports or active media. Zeolite films can be suitable for catalytic membrane reactors.[40] The specific uses of zeolite film applications indicated in the literature[41] are plate reactors and that preparation of *b*-oriented zeolite films/membranes can improve mass transfer efficiency and enhance the selectivity of products, catalytic activity, and catalyst stability.[42] One study has described the processing of layer-based materials (the $[Ru(bpy)_3]^{2+}$–TiO_2@clay nanoarchitecture) as a film to be mounted in a flow reactor.[43]

Conclusions

A recently reported method for the exfoliation of zeolites to produce a solution of unilamellar nanosheets[21,22] is extended to the layered zeolite MFI, which is the most important framework available as a modifiable layer that is also permeable. The as-synthesized material was calcined at 350 °C, to degrade the template covering the surface, and treated with TBAOH. Solids were purified by high-speed centrifugation. The presence of unilamellar MFI nanosheets in the obtained solutions has been proven by AFM, in-plane XRD, TEM microscopy, and flocculation with organic compounds. The nanosheets produced oriented discs and films. They maintained the original acid and textural properties and thus are suitable for catalytic and sorption applications.

The reported direct exfoliation provides a simpler alternative to some of the previously published methods for producing zeolite films and membranes, which usually started with surfactant-expanded layered precursors.[23,29] Zeolite membrane preparation and testing are difficult and challenging tasks that require special equipment, expertise and skills.[25,44] Consequently, the development and evaluation of the potential presented by the current exfoliation approach in the area of membrane separation will require separate dedicated efforts.

Experimental methods

Synthesis of the template and layered MFI

The template (SDA) with the formula $RN(CH_2)_nNC_mH_{2m+1}Br_2$, R – $C_{22}H_{45}$, n and m = 6, designated C22-6-6, was prepared as reported earlier.[32]

N,*N*,*N*′,*N*′-Tetramethyl-1,6-diaminohexane (61.7 g, 0.357 mL, from TCI) and 1-bromodocosane (19.9 g, 0.051 mol, TCI) were dissolved in toluene/acetonitrile (300 mL, 1 : 1 vol/vol) and heated at 65 °C for 20 h. After cooling to room temperature, the product was filtered, washed with cold diethyl ether, and dried in an oven at 60 °C. This product (27.2 g, 0.048 mol) was combined with 1-bromohexane (12.0 g, 0.073 mol, from Aldrich) dissolved in acetonitrile (200 mL) and refluxed at 65 °C for 8 h. After cooling to room temperature, the product was filtered, washed with cold diethyl ether, and dried in a vacuum oven at 60 °C.

The first MFI sample was prepared with the gel Si/Al ratio of 29/1 by mixing water (8.4 g), 50% NaOH (0.31 g), aluminium nitrate nonahydrate (0.21 g) and tetraethyl orthosilicate (TEOS, 3.3 g), all reagents from Sigma Aldrich, and adding the above C22-6-6 template (1.1 g). After rotation overnight, the mixture was heated at 150 °C with rotation for 110 h, sampled and reheated for additional 16 h. The as-synthesized product was isolated by filtration, washed with water, and dried in air.

The second MFI sample with gel Si/Al = 23/1 was prepared like above with the following corresponding weights of reagents: water (8.72 g), 50% NaOH (0.32 g), aluminium nitrate nonahydrate (0.255 g), TEOS (3.315 g) and the template (1.137 g). The synthesis time was 102 h with one sampling at 92 h.

The as-synthesized zeolite was calcined at 350 °C for 10 h with 10 h ramp to the holding temperature. The product was red-brown and was first treated (1–1.5 g) with 20 mL of 10% tetrabutylammonium hydroxide (TBAOH, Sigma Aldrich), stirred for 1.5–2 h, centrifuged for >30 min at 10 000 rpm until well settled. The red-brown supernatant was decanted and discarded. The solid was mixed with 30 g of water, stirred for 1.5 to 20 h and centrifuged at 10 000 rpm; *ca.* 25 mL of the supernatant was pipetted out and preserved, while the rest including solid was mixed with water again and the sequence was repeated 3–4 times, providing several solutions with exfoliated zeolite MFI layers. If needed, the nanosheets were flocculated by acidification with 1 M HCl, and the solids were isolated by centrifugation, combined or used separately. The flocculated layers can be re-dispersed by stirring with a few mililitres of 0.02 M TBAOH (*ca.* 0.5%).

Basic characterization by X-ray powder diffraction, nitrogen adsorption, FTIR and TG-DTG

Powder XRD patterns were collected using a Bruker AXS D8 Advance diffractometer equipped with a graphite monochromator and a position sensitive detector (Våntec-1) in the Bragg–Brentano geometry and a Rigaku MiniFlex diffractometer in the reflection mode. The radiation source was CuKα with λ = 0.154 nm. The typical XRD step size was equal to a 2θ value of 0.02° and the scan was at a 2θ value of 2.0° or less per minute.

Discs were mounted on a special silicon holder and pressed to the surface with a transparent plastic film (both showing reflections in the XRD in the 2θ region of 25–30°).

Nitrogen adsorption/desorption isotherms were measured on a Micromeritics 3Flex volumetric surface area analyzer at −196 °C. Before the sorption measurements, all samples were outgassed under the turbomolecular pump vacuum using a Micromeritics Smart Vac Prep instrument; starting at an ambient temperature up to 110 °C with a heating rate of 1 °C min^{-1} until the residual pressure of 13.3 Pa was achieved. After heating at 110 °C for 1 h, the temperature was increased to 250 °C (1 °C min^{-1}) and maintained for 8 h.

 This journal is © the Partner Organisations 2023

Open Access Article. Published on 27 Januar 2023. Downloaded on 09.10.2025 04:40:51.
This article is licensed under a Creative Commons Attribution 3.0 Unported Licence.

FTIR measurements of the acid site concentrations were carried out by the adsorption of pyridine (Py) followed by IR spectroscopy using Tensor 27 from Bruker, an MCT detector, and a spectral resolution of 2 cm^{-1}. Calcined samples were exchanged with an excess of 1 M ammonium nitrate solution (>10 : 1), dried at 110 °C and pressed into self-supporting wafers with a density of *ca.* 8 mg cm^{-2}. They were activated *in situ* at 450 °C for 1 h at high vacuum (10^{-5} mbar). Excess of pyridine vapor (*ca.* 20 mbar equilibrium pressure) was adsorbed at 170 °C followed by desorption for 20 min at the adsorption temperature. Spectra were recalculated to a wafer mass equal 10 mg. Concentrations of Lewis (LAS) and Brønsted (BAS) acid sites were evaluated from the intensities of bands at 1454 cm^{-1} (LAS) and at 1545 cm^{-1} (BAS) using absorption coefficients, determined earlier in our laboratory using external standards ε(LAS) = 0.165 cm^2 μmol^{-1}, and ε(BAS) = 0.044 cm^2 μmol^{-1},[45] and the intensities of corresponding pyridine maxima after pyridine desorption at 170 °C to ensure the complete removal of weakly adsorbed species. Discs were mounted in a holder and examined as above.

The TG-DTG measurement was carried out with the TGA/DSC 3+ instrument (Mettler Toledo, Greifensee, Switzerland). The TG and DTG profiles were obtained under a flow of synthetic air (80 mL min^{-1}), with a linear temperature increase of 10° per min in the temperature range of 30–1100 °C.

Atomic force microscopy

Branched polyethyleneimine (PEI, $M_w \sim 600$ g mol^{-1}) was purchased from Sigma Aldrich. Ethanol (p.a.) and NaCl (p.a.) were purchased from Chempur. All regents were used as received.

Silicon wafer substrates were cleaned first by sonication in ethanol for 10 min and then rinsed with ethanol, dried in a stream of argon, and treated in a UV-ozone cleaner for 30 min. Such cleaned substrates were placed in glass vials with a PEI solution (concentration 1 g dm^{-3}) in 0.01 M NaCl. The PEI deposition was supported by pulse sonication (15 min). After completion, the supports were rinsed with copious amounts of deionized water and dried in a stream of argon. An MFI nanosheet solution was spin-cast at 2 000 rpm for 120 s on the PEI modified supports. Atomic force microscopy (AFM) images were obtained with a Dimension Icon AFM (Bruker, Santa Barbara, CA) working in the PeakForce Tapping® (PFT) and QNM® modes. The probes were RTESPA-150 (Bruker, nominal spring constant: 5 N m^{-1}, nominal tip radius: 8 nm), were used in the measurements. The AFM topography images were captured in air with a total resolution of 384 × 384 pixels.

In-plane XRD

The layers flocculated by HCl from the nanosheet solution obtained from the second (23/1 Si/Al) preparation were redissolved in 0.5% TBAOH. The specimens were prepared by depositing the nanosheets from their suspension on a Si substrate through the Langmuir–Blodgett method (surface compression at 11 mN m^{-1} and lifting speed at 1 mm min^{-1}), described in detail elsewhere.[46,47]

XRD data were collected using synchrotron radiation X-rays (λ = 0.11987(2) nm) at Photon Factory, BL-6C, KEK. The baseline at a low angular range was removed and peaks having a FWHM of ~0.2° 2θ (λ = 0.11987(2) nm) were selected by the standard software.

TEM

The structure of the MFI nanosheets was characterized by TEM, using a JEM-ARM200F (accelerating voltage, 80 kV) equipped with a Cs image corrector (CEOS). A solution with MFI nanosheets was diluted 50-fold and dropped on a carbon-coated grid to prepare the TEM specimen. The images and selective area electron diffraction (SAED) patterns were recorded with a Gatan OneView and a Gatan Orius CCD camera, respectively.

STEM and SEM

STEM images were acquired using a JEOL NEOARM 200F atomic resolution analytical electron microscope operating at 200 kV, using ABF and ADF detectors. For STEM, a sample was crushed before the measurement to reduce the size to meet requirements for the transmission electron microscopy.

SEM imaging of the discs was performed using a JEOL IT-800 HR-SEM secondary electrons (SE) detector. The scanning electron microscope (SEM) images of the original MFI presented in Fig. S2† were collected with a VEGA 3 TESCAN with a LaB_6 cathode. The measurements were performed on a carbon sheet with gold sputtering.

Author contributions

WJR – conceptualization, investigation, supervision, writing – original draft, and review and editing; ST – conceptualization, investigation, supervision, writing – review and editing; BG – investigation, supervision, writing – review and editing; SZ, RM – investigation and supervision; JC – conceptualization, supervision, writing – review and editing; KW, MK, MM, YE, NS, D-MT – investigation and writing.

Conflicts of interest

There are no conflicts to declare.

Acknowledgements

This work was financed with the funds from the National Science Centre Poland, grant no 2020/37/B/ST5/01258 (WJR, BG). The in-plane XRD measurements were performed under the approval of the Photon Factory Program Advisory Committee (Proposal No. 2020G503). JC and MK acknowledge the Czech Science Foundation for funding this research through the ExPro project (19-27551X). MM and JC acknowledge OP VVV "Excellent Research Teams", project no. CZ.02.1.01/0.0/0.0/15_003/0000417 – CUCAM. The authors also

thank the Laboratory of Electron Microscopy, Imaging Methods Core Facility of Biology Section, Faculty of Science (IMCF Viničná) for SEM access. TS acknowledges the Japan Science and Technology Agency (JST), Grant No. JPMJCR17N1 (CREST) and the Japan Society for the Promotion of Science (JSPS), Grant No. P21036. The open-access publication of this article was funded by the program "Excellence Initiative – Research University" at the Jagiellonian University in Kraków.

Open Access Article. Published on 27 Januar 2023. Downloaded on 09.10.2025 04:40:51.
This article is licensed under a Creative Commons Attribution 3.0 Unported Licence.

References

1 M. E. Davis, Zeolites and molecular-sieves - not just ordinary catalysts, *Ind. Eng. Chem. Res.*, 1991, **30**, 1675–1683.
2 P. Van Der Voort, K. Leus and E. De Canck, *Introduction to porous materials*, Wiley, Hoboken, NJ, 2019.
3 J. Rouquerol, F. Rouquerol, P. Llewellyn, G. Maurin and K. S. W. Sing, *Adsorption by Powders and Porous Solids: Principles, Methodology and Applications*, Elsevier Science, 2013.
4 C. Martinez and A. Corma, Inorganic molecular sieves: Preparation, modification and industrial application in catalytic processes, *Coord. Chem. Rev.*, 2011, **255**, 1558–1580.
5 C. S. Cundy and P. A. Cox, The hydrothermal synthesis of zeolites: History and development from the earliest days to the present time, *Chem. Rev.*, 2003, **103**, 663–701.
6 A. Primo and H. Garcia, Zeolites as catalysts in oil refining, *Chem. Soc. Rev.*, 2014, **43**, 7548–7561.
7 I. Fechete, Y. Wang and J. C. Védrine, The Past, Present and Future of Heterogeneous Catalysis, *Catal. Today*, 2012, **189**, 2–27.
8 A. F. Masters and T. Maschmeyer, Zeolites - From curiosity to cornerstone, *Microporous Mesoporous Mater.*, 2011, **142**, 423–438.
9 I. Fechete and J. C. Vedrine, Nanoporous Materials as New Engineered Catalysts for the Synthesis of Green Fuels, *Molecules*, 2015, **20**, 5638–5666.
10 L. Wang and F. S. Xiao, Nanoporous catalysts for biomass conversion, *Green Chem.*, 2015, **17**, 24–39.
11 S. I. Zones, Translating new materials discoveries in zeolite research to commercial manufacture, *Microporous Mesoporous Mater.*, 2011, **144**, 1–8.
12 M. E. Leonowicz, J. A. Lawton, S. L. Lawton and M. K. Rubin, MCM-22 - A Molecular Sieve with 2 Independent Multidimensional Channel Systems, *Science*, 1994, **264**, 1910–1913.
13 M. K. Rubin and P. Chu, Composition of Synthetic Porous Crystalline Material, Its Synthesis and Use, *US Pat*, 4954325, 1990.
14 L. Schreyeck, P. Caullet, J.-C. Mougenel, J.-L. Guth and B. Marler, A layered microporous aluminosilicate precursor of FER-type zeolite, *J. Chem. Soc., Chem. Commun.*, 1995, 2187–2188.
15 S. L. Lawton, A. S. Fung, G. J. Kennedy, L. B. Alemany, C. D. Chang, G. H. Hatzikos, D. N. Lissy, M. K. Rubin, H. K. C. Timken, S. Steuernagel and D. E. Woessner, Zeolite MCM-49: A Three-Dimensional MCM-22 Analogue Synthesized by in situ Crystallization, *J. Phys. Chem.*, 1996, **100**, 3788–3798.
16 B. Marler and H. Gies, Hydrous Layer Silicates as Precursors for Zeolites Obtained through Topotactic Condensation: A Review, *Eur. J. Mineral.*, 2012, **24**, 405–428.
17 W. J. Roth, C. T. Kresge, J. C. Vartuli, M. E. Leonowicz, A. S. Fung and S. B. McCullen, MCM-36: The First Pillared Molecular Sieve with Zeolite Properties, *Stud. Surf. Sci. Catal.*, 1995, **94**, 301–308.
18 M. Opanasenko, W. Roth and J. Cejka, Two-dimensional zeolites in catalysis: current status and perspectives, *Catal. Sci. Technol.*, 2016, **6**, 2742–2753.
19 E. Schulman, W. Wu and D. X. Liu, Two-Dimensional Zeolite Materials: Structural and Acidity Properties, *Materials*, 2020, **13**, 1822.
20 W. J. Roth, P. Nachtigall, R. E. Morris and J. Čejka, Two-dimensional zeolites: current status and perspectives, *Chem. Rev.*, 2014, **114**, 4807–4837.
21 W. J. Roth, T. Sasaki, K. Wolski, Y. Ebina, D. M. Tang, Y. Michiue, N. Sakai, R. Z. Ma, O. Cretu, J. Kikkawa, K. Kimoto, K. Kalahurska, B. Gil, M. Mazur, S. Zapotoczny, J. Cejka, J. Grzybek and A. Kowalczyk, Exfoliated Ferrierite-Related Unilamellar Nanosheets in Solution and Their Use for Preparation of Mixed Zeolite Hierarchical Structures, *J. Am. Chem. Soc.*, 2021, **143**, 11052–11062.
22 W. J. Roth, T. Sasaki, K. Wolski, Y. Song, D. M. Tang, Y. Ebina, R. Z. Ma, J. Grzybek, K. Kalahurska, B. Gil, M. Mazur, S. Zapotoczny and J. Cejka, Liquid dispersions of zeolite monolayers with high catalytic activity prepared by soft-chemical exfoliation, *Sci. Adv.*, 2020, **6**, eaay8163.
23 K. Varoon, X. Y. Zhang, B. Elyassi, D. D. Brewer, M. Gettel, S. Kumar, J. A. Lee, S. Maheshwari, A. Mittal, C. Y. Sung, M. Cococcioni, L. F. Francis, A. V. McCormick, K. A. Mkhoyan and M. Tsapatsis, Dispersible Exfoliated Zeolite Nanosheets and Their Application as a Selective Membrane, *Science*, 2011, **334**, 72–75.
24 M. Shamzhy, B. Gil, M. Opanasenko, W. J. Roth and J. Čejka, MWW and MFI Frameworks as Model Layered Zeolites: Structures, Transformations, Properties, and Activity, *ACS Catal.*, 2021, **11**, 2366–2396.
25 K. V. Agrawal, Towards the Ultimate Membranes: Two-dimensional Nanoporous Materials and Films, *Chimia*, 2018, **72**, 313–321.
26 S. Sabnis, V. A. Tanna, C. Li, J. X. Zhu, V. Vattipalli, S. S. Nonnenmann, G. Sheng, Z. P. Lai, H. H. Winter and W. Fan, Exfoliation of two-dimensional zeolites in liquid polybutadienes, *Chem. Commun.*, 2017, **53**, 7011–7014.
27 V. Nicolosi, M. Chhowalla, M. G. Kanatzidis, M. S. Strano and J. N. Coleman, Liquid Exfoliation of Layered Materials, *Science*, 2013, **340**, 1–18.
28 A. Corma, V. Fornes, S. B. Pergher, T. L. M. Maesen and J. G. Buglass, Delaminated Zeolite Precursors as Selective Acidic Catalysts, *Nature*, 1998, **396**, 353–356.

 This journal is © the Partner Organisations 2023

Open Access Article. Published on 27 Januar 2023. Downloaded on 09.10.2025 04:40:51.
This article is licensed under a Creative Commons Attribution 3.0 Unported Licence.

29 M. Dakhchoune, L. F. Villalobos, R. Semino, L. M. Liu, M. Rezaei, P. Schouwink, C. E. Avalos, P. Baade, V. Wood, Y. Han, M. Ceriotti and K. V. Agrawal, Gas-sieving zeolitic membranes fabricated by condensation of precursor nanosheets, *Nat. Mater.*, 2021, **20**, 362–369.

30 P. Loch, D. Schuchardt, G. Algara-Siller, P. Markus, K. Ottermann, S. Rosenfeldt, T. Lunkenbein, W. Schwieger, G. Papastavrou and J. Breu, Nematic suspension of a microporous layered silicate obtained by forceless spontaneous delamination via repulsive osmotic swelling for casting high-barrier all-inorganic films, *Sci. Adv.*, 2022, **8**, eabn9084.

31 N. Rangnekar, N. Mittal, B. Elyassi, J. Caro and M. Tsapatsis, Zeolite membranes - a review and comparison with MOFs, *Chem. Soc. Rev.*, 2015, **44**, 7128–7154.

32 M. Choi, K. Na, J. Kim, Y. Sakamoto, O. Terasaki and R. Ryoo, Stable Single-Unit-Cell Nanosheets of Zeolite MFI as Active and Long-Lived Catalysts, *Nature*, 2009, **461**, 246–249.

33 D. Kim, M. Shete and M. Tsapatsis, Large-Grain, Oriented, and Thin Zeolite MFI Films from Directly Synthesized Nanosheet Coatings, *Chem. Mater.*, 2018, **30**, 3545–3551.

34 W. Park, D. Yu, K. Na, K. E. Jelfs, B. Slater, Y. Sakamoto and R. Ryoo, Hierarchically Structure-Directing Effect of Multi-Ammonium Surfactants for the Generation of MFI Zeolite Nanosheets, *Chem. Mater.*, 2011, **23**, 5131–5137.

35 H. Van Koningsveld, J. C. Jansen and H. Van Bekkum, The monoclinic framework structure of zeolite H-ZSM-5. Comparison with the orthorhombic framework of as-synthesized ZSM-5, *Zeolites*, 1990, **10**, 235–242.

36 Z. Wang, T. Yu, P. Nian, Q. Zhang, J. Yao, S. Li, Z. Gao and X. Yue, Fabrication of a Highly b-Oriented MFI-Type Zeolite Film by the Langmuir–Blodgett Method, *Langmuir*, 2014, **30**, 4531–4534.

37 W. J. Roth and C. T. Kresge, Intercalation chemistry of NU-6(1), the layered precursor to zeolite NSI, leading to the pillared zeolite MCM-39(Si), *Microporous Mesoporous Mater.*, 2011, **144**, 158–161.

38 K. Ufer, H. Stanjek, G. Roth, R. Dohrmann, R. Kleeberg and S. Kaufhold, Quantitative phase analysis of bentonites by the Rietveld method, *Clays Clay Miner.*, 2008, **56**, 272–282.

39 W. J. Roth, J. Čejka, R. Millini, E. Montanari, B. Gil and M. Kubu, Swelling and interlayer chemistry of layered MWW zeolites MCM-22 and MCM-56 with high Al content, *Chem. Mater.*, 2015, **27**, 4620–4629.

40 J. Jiang, M. Zhu, Y. Liu, Y. Li, T. Gui, N. Hu, F. Zhang, X. Chen and H. Kita, Influences of synthesis conditions on preparation and characterization of Ti-MWW zeolite membrane by secondary hydrothermal synthesis, *Microporous Mesoporous Mater.*, 2020, **297**, 110004.

41 Y. C. Li, G. F. Zhu, Y. Wang, Y. M. Chai and C. G. Liu, Preparation, mechanism and applications of oriented MFI zeolite membranes: A review, *Microporous Mesoporous Mater.*, 2021, **312**, 110790.

42 Y. Sun, S. Cao, J. Wang, H. Tang, Z. Yang, T. Ma, Y. Gong, G. Mo and Z. Li, Fabrication of Twin-Free Nanoslab ZSM-5 Zeolite with b-Axis Orientation for Super MTP Catalyst, *ACS Sustainable Chem. Eng.*, 2022, **10**, 9431–9442.

43 E. Ruiz-Hitzky, P. Aranda, M. Akkari, N. Khaorapapong and M. Ogawa, Photoactive nanoarchitectures based on clays incorporating TiO2 and ZnO nanoparticles, *Beilstein J. Nanotechnol.*, 2019, **10**, 1140–1156.

44 M. Y. Jeon, D. Kim, P. Kumar, P. S. Lee, N. Rangnekar, P. Bai, M. Shete, B. Elyassi, H. S. Lee, K. Narasimharao, S. N. Basahel, S. Al-Thabaiti, W. Xu, H. J. Cho, E. O. Fetisov, R. Thyagarajan, R. F. DeJaco, W. Fan, K. A. Mkhoyan, J. I. Siepmann and M. Tsapatsis, Ultra-selective high-flux membranes from directly synthesized zeolite nanosheets, *Nature*, 2017, **543**, 690.

45 A. Korzeniowska, J. Grzybek, K. Kalahurska, M. Kubu, W. J. Roth and B. Gil, The structure-catalytic activity relationship for the transient layered zeolite MCM-56 with MWW topology, *Catal. Today*, 2020, **345**, 116–124.

46 M. Muramatsu, K. Akatsuka, Y. Ebina, K. Wang, T. Sasaki, T. Ishida, K. Miyake and M.-A. Haga, Fabrication of Densely Packed Titania Nanosheet Films on Solid Surface by Use of Langmuir–Blodgett Deposition Method without Amphiphilic Additives, *Langmuir*, 2005, **21**, 6590–6595.

47 T. Shibata, K. Fukuda, Y. Ebina, T. Kogure and T. Sasaki, One-Nanometer-Thick Seed Layer of Unilamellar Nanosheets Promotes Oriented Growth of Oxide Crystal Films, *Adv. Mater.*, 2008, **20**, 231–235.